

RESEARCH

Open Access



Paraspinal myosteatosi s is associated with COPD: a cross-sectional MRI analysis from the population-based KORA cohort

Thierno D. Diallo^{1*}, Stefan Karrasch^{2,3,4}, Matthias Jung¹, Annette Peters^{4,5}, Roberto Lorbeer⁶, Christopher L. Schlett¹, Ricarda von Krüchten¹, Fabian Bamberg¹, Susanne Rospleszcz^{1,4} and Lena S. Kiefer^{7,8}

Abstract

Background Muscle dysfunction in chronic obstructive pulmonary disease (COPD) represents a significant extrapulmonary manifestation. Yet, the role of muscle fat infiltration (myosteatosi s) in paraspinal muscles remains incompletely characterized. This study investigated whether paraspinal myosteatosi s and its distribution patterns are associated with COPD and pulmonary function.

Methods Within the population-based KORA cohort, 214 participants underwent whole-body magnetic resonance imaging and pulmonary function testing. Paraspinal myosteatosi s was quantified by chemical shift-encoded MRI at lumbar vertebra 3 (L3), from which proton density fat fraction (PDFF, in %) maps were derived. Intramyocellular (IMCL) and extramyocellular lipids (EMCL) were determined through voxel-based analysis using validated PDFF thresholds. COPD was defined spirometrically as FEV1/FVC below the lower limit of normal. Associations were examined using multivariable regression models adjusted for age, sex, smoking status, physical activity, and body mass index.

Results Among participants (mean age 58.5 ± 5.8 years, 56.1% male), 24 (11.2%) had spirometrically defined COPD. Participants with COPD showed higher paraspinal PDFF (19.9 ± 7.0% vs. 18.3 ± 7.6%) and lower IMCL/EMCL ratios (1.0 ± 0.4 vs. 1.2 ± 0.6) compared to those without COPD. After adjustment, higher PDFF was independently associated with increased odds of COPD (OR 1.69, 95% CI: 1.01–2.84, *p* = 0.046), while a higher IMCL to EMCL ratio showed protective associations (OR 0.49, 95% CI: 0.24–1.00, *p* = 0.050). Both total paraspinal PDFF and EMCL were negatively associated with pulmonary gas exchange capacity (TLCO/VA: β = -0.19, 95% CI: -0.35–0.04, *p* = 0.016 and β = -0.18, 95% CI: -0.33–0.03, *p* = 0.022, respectively). Conversely, higher IMCL/EMCL ratios were associated with better gas exchange (TLCO/VA: β = 0.15, 95% CI: 0.01–0.29, *p* = 0.031).

Conclusions This population-based study demonstrates that while increased total paraspinal muscle fat content is associated with higher COPD risk, its compartmental distribution reveals distinct patterns: A higher proportion of IMCL relative to EMCL shows protective associations, potentially reflecting preserved type I oxidative muscle fiber characteristics. These findings suggest that muscle fat distribution patterns may serve as imaging markers of metabolic adaptation in COPD, offering new perspectives for disease monitoring and therapeutic approaches.

*Correspondence:

Thierno D. Diallo
thierno.diallo@uniklinik-freiburg.de

Full list of author information is available at the end of the article



© The Author(s) 2025. **Open Access** This article is licensed under a Creative Commons Attribution 4.0 International License, which permits use, sharing, adaptation, distribution and reproduction in any medium or format, as long as you give appropriate credit to the original author(s) and the source, provide a link to the Creative Commons licence, and indicate if changes were made. The images or other third party material in this article are included in the article's Creative Commons licence, unless indicated otherwise in a credit line to the material. If material is not included in the article's Creative Commons licence and your intended use is not permitted by statutory regulation or exceeds the permitted use, you will need to obtain permission directly from the copyright holder. To view a copy of this licence, visit <http://creativecommons.org/licenses/by/4.0/>.

Keywords Myosteatosi s, Obstructive lung disease, Body composition, Magnetic resonance imaging, Imaging biomarker

Introduction

Chronic obstructive pulmonary disease (COPD) represents a significant health burden, and is considered a leading cause of morbidity and mortality worldwide [1]. It is characterized by chronic airflow obstruction leading to impaired pulmonary function, with profound effects on gas exchange and respiratory mechanics [2]. Beyond pulmonary manifestations, individuals with COPD often exhibit systemic effects, with skeletal muscle dysfunction being a key feature that substantially impacts functional status and quality of life [3]. Muscle dysfunction in COPD can manifest as decreased muscle strength, endurance, and mass [4]. While the loss of muscle mass (sarcopenia) has been extensively studied in respiratory diseases [5, 6], the role of muscle fat infiltration (myosteatosi s) remains less well characterized. Myosteatosi s represents qualitative muscle alterations that affect tissue architecture and metabolic function. It can manifest independently of sarcopenia and may even precede muscle mass loss [7]. In skeletal muscle, fat can accumulate as intramyocellular lipids (IMCL), stored as lipid droplets within muscle fibers serving as physiological energy substrates during oxidative metabolism particularly in type I fibers, and as extramyocellular lipids (EMCL). EMCL represent ectopic fat depots stored in adipocytes, either between muscle fibers within individual muscles (intramuscular), between muscles and their fascia or between muscle groups (both intermuscular) [8, 9]. Intermuscular adipose tissue, acts as an endocrine organ producing inflammatory mediators that can directly affect skeletal muscle metabolism [10, 11]. Consequently, not only the total amount of muscle fat but also its distribution between intra- and extramyocellular compartments may provide insights into muscle metabolism and function.

Chemical shift encoded magnetic resonance imaging (MRI) provides a non-invasive method for detailed assessment of muscle mass and quantitative evaluation of myosteatosi s while allowing the differentiation of IMCL and EMCL compartments [12]. Several studies have established myosteatosi s as an important prognostic marker across various conditions and as a strong predictor of all-cause mortality in both individuals with metabolic disorders and asymptomatic adults [7, 13–15].

Despite evidence linking muscle dysfunction with COPD, the associations between MRI-derived muscle parameters, especially myosteatosi s, and COPD in the general population remain underexplored. Therefore, we investigated associations between paraspi nal myosteatosi s and its distribution in relation to spirometrically defined COPD in a sample of adults

from a population-based cohort. We hypothesized that increased muscle fat content would be associated with increased prevalence of COPD, and that IMCL and EMCL would demonstrate different associations with COPD and related respiratory parameters.

Materials and methods

Study sample

We used data from the cross-sectional MRI substudy within the “Cooperative Health Research in the Region of Augsburg” (KORA) cohorts [16]. The MRI examination was done within the second follow-up KORA-FF4 ($N=2279$, enrolled in 2013/2014) of the original population-based KORA-S4 survey ($N=4261$, enrolled in 1999/2001). Of the KORA-FF4 cohort, $N=400$ participants underwent whole-body MRI within 33 days (interquartile range: 24–45 days) of their examination at the study center. Inclusion criteria were no contraindications to MRI (claustrophobia, allergy to contrast agent, permanent metal parts in the body), age < 74 years, being in generally good health sufficient for the one-hour whole-body imaging procedure, and no prevalent cardiovascular disease (stroke, myocardial infarction, revascularization) [16]. Additionally, $N=1010$ participants of the KORA-FF4 cohort in the age range 48–68 years underwent pulmonary function testing [17]. The overlap of these two samples constitutes the analytical sample for the current analysis. The Ethics committee of the Bavarian Chamber of Physicians approved the general KORA cohort studies. The Ethics Committee of the Ludwig-Maximilians University Munich (Munich, Germany) additionally approved the whole-body MRI substudy (No. 498–12). The study was carried out in accordance with the Declaration of Helsinki and obtained written informed consent from all participants. Clinical trial number: not applicable.

MRI protocol and muscle segmentation

MRI examinations were performed using a 3 Tesla Magnetom Skyra scanner (Siemens Healthineers, Erlangen, Germany) with combined 18-channel body surface and spine matrix coils. The complete imaging protocol and technical specificities have been described in detail previously [16]. For muscle analysis, T2*-corrected multi-echo 3D-gradient-echo Dixon sequences of the upper abdomen were acquired during a single breath-hold (slice thickness 4 mm, voxel size 1.8×1.8 mm, field-of-view 393×450 mm, matrix 256×179 , TR 8.90ms, TE s 1.23, 2.46, 3.69, 4.92, 6.15, 7.38ms, flip angle 4°). Accurate transverse slice positioning at L3 vertebral level was

confirmed using coronal two-point Dixon gradient-echo sequences (TR 4.06ms, TE 1.26 and 2.49ms, flip angle 9°, slice thickness 1.7 mm, isotropic in-plane resolution 1.7 mm) with cross-reference. Paraspinal muscles were manually segmented at the level of the third lumbar vertebra by two observers blinded to clinical data and COPD status using standardized anatomical landmarks (MITK V2015.5.2, German Cancer Research Center, Heidelberg, Germany). Skeletal muscle area (mm²) was defined as the sum of the left and right areas of the paraspinal muscles (Fig. 1).

Myosteatorsis quantification

Total myosteatorsis was determined as proton density fat fraction (PDFF, in %). PDFF maps were calculated from the original data using the manufacturer's software (MR Liverlab, Version VD13, Siemens Healthineers, Cary, USA). Mean PDFF was calculated by averaging measurements from right and left muscle compartments, including IMCL, intramuscular and subfascial intermuscular EMCL, while excluding surrounding extrafascial intermuscular EMCL. The reproducibility of this segmentation approach was previously validated in a methodological study using the same protocol, demonstrating excellent reliability with intraclass correlation coefficients of 0.98 and 0.99 for inter- and intra-observer agreement of PDFF measurements, and 0.97 and 0.98 for muscle area measurements [18].

For differentiation of fat compartments, IMCL were quantified by postprocessing the segmented muscle compartments using a semi-automated algorithm (Matlab_R2017a; MathWorks, MA, USA). This algorithm applies an established threshold based on the understanding that myocytes with high intramyocellular lipid content demonstrate values $\leq 20\%$, while higher values indicate the presence of extramyocellular adipose tissue [12]. This 20% PDFF threshold follows the physiological rationale, where values below 20% reflect small intracellular lipid droplets and above 20% larger adipocyte aggregates [19]. Accordingly, voxels with PDFF values $\leq 20\%$ were classified as containing IMCL, while EMCL content was calculated as the difference between total paraspinal myosteatorsis and IMCL, comprising predominantly extramyocellular intramuscular fatty septa and subfascial intermuscular adipose tissue [18].

Pulmonary function testing

As reported previously [20], three categories of pulmonary function indices were analyzed: (1) Spirometric indices including forced vital capacity (FVC), forced expiratory volume in 1 s (FEV1), FEV1/FVC, and forced expiratory flow between 25% and 75% of FVC (FEF25–75); (2) lung volumes derived from single-breath measurement of pulmonary gas exchange, which include residual volume (RV), functional residual capacity (FRC), total lung capacity (TLC), and alveolar volume (VA); (3)

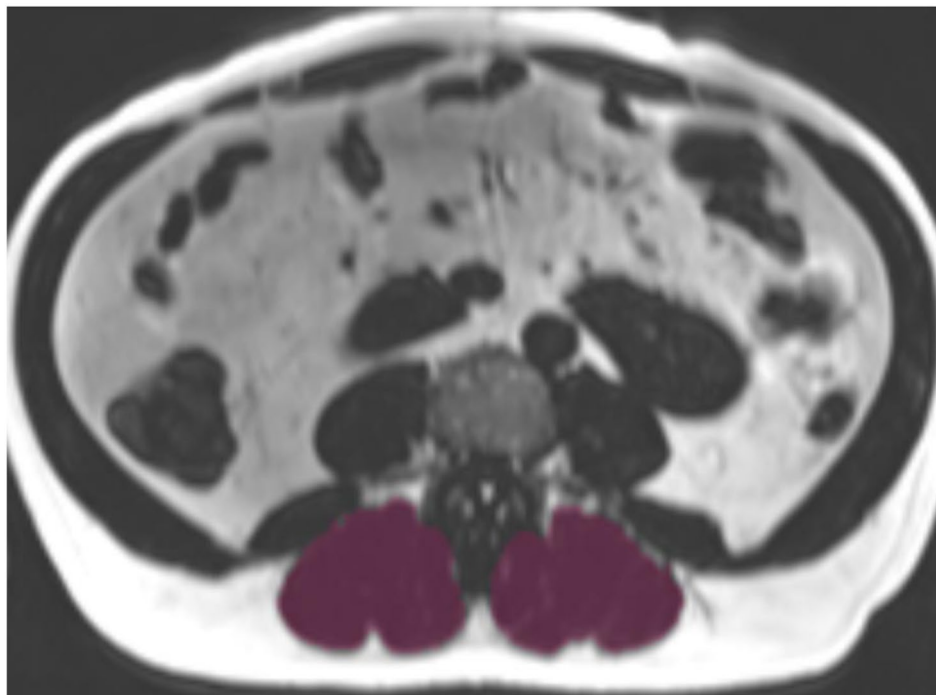


Fig. 1 Representative axial T2*-corrected multi-echo Dixon MRI slice (fat contrast) at level L3 with superimposed paraspinal muscle segmentation (purple). Manual segmentation was performed bilaterally using standardized anatomical landmarks

Abbreviations: MRI: magnetic resonance imaging; L3: 3rd lumbar vertebra

indices of pulmonary gas exchange, which include transfer factor of the lung for carbon monoxide (TLCO) and the transfer coefficient TLCO/VA. Standard spirometry without bronchodilation and single-breath measurement of TLCO were performed in line with German as well as American Thoracic Society (ATS)/European Respiratory Society (ERS) recommendations in upright sitting position using a pneumotachograph-type spirometer (MasterScope PC and MasterScreen PFT, CareFusion, Höchberg, Germany) [21]. At least three and up to eight spirometric maneuvers and up to five single-breath TLCO maneuvers were performed to obtain a minimum of two acceptable and reproducible measurements. COPD was defined as FEV1/FVC below the Lower Limit of Normal (LLN) based on American Thoracic Society and European Respiratory Society recommendations using Global Lung Initiative reference values that are based on age, sex, height and ethnicity [22, 23].

Clinical covariates

All participants underwent standardized interviews and physical examinations at the study center. Anthropometric measurements, including weight, height, and body mass index (BMI), were obtained according to standardized protocols. Blood pressure measurements were performed to assess hypertension, defined as systolic blood pressure ≥ 140 mmHg, diastolic blood pressure ≥ 90 mmHg, or current antihypertensive medication. Laboratory analysis of fasting blood samples included the determination of blood lipid parameters (HDL, LDL, and triglycerides) and inflammatory markers (hsCRP) by standard laboratory measures. Smoking behavior was assessed by self-report and classified into never, former and current smoker. Study participants were classified as physically active (regular physical activity ≥ 2 h/week or approximately 1 h/week) or physically inactive (irregular physical activity < 1 h/week, almost no or no physical activity), based on self-report.

Statistical methods

Participants' baseline characteristics for the whole sample and stratified by COPD status are presented as mean and standard deviation or median with interquartile range for continuous data, and counts and percentages for categorical data. Differences between groups were quantified by t-test or Wilcoxon-test, and χ^2 test or Fisher's exact test for groups with $n < 5$, respectively.

Univariate correlations between MRI-derived skeletal muscle parameters and pulmonary function were quantified by Spearman's correlation coefficient.

To evaluate the association between MRI-derived skeletal muscle parameters as exposure and pulmonary function parameters as an outcome, adjusted linear and logistic regression models were applied. Models were

adjusted for 1) age and sex, 2) age, sex, smoking, diabetes, physical activity (yes/no), and BMI, and 3) Model 2 plus hsCRP. All exposures and continuous outcomes were centered and scaled (minus mean and divided by standard deviation) before modelling. Results are given as beta coefficients or Odds Ratios (OR) with respective 95% confidence intervals.

R version 4.4.1 was used for statistical analysis. *P*-values < 0.05 were considered to denote statistical significance of associations, without adjustment for multiple testing.

Results

Study sample

Of the $N = 400$ individuals originally enrolled in KORA-MRI, one retroactively withdrew consent for data usage, $n = 174$ did not undergo pulmonary function testing, and $n = 11$ had no data on skeletal muscle area and PDFF from MRI. Therefore, the final analytical sample comprised $N = 214$ participants (Fig. 2), with varying sample sizes for some variables (Table 1).

Individuals of the original KORA-MRI sample that were excluded from the current analysis were, on average, younger and had lower cardiometabolic risk factor levels (Supplementary Table 1). Individuals in the sample were 58.5 ± 5.8 years old, 56.1% were men, and 21% were active smokers (Table 1). COPD, as defined by LLN, was present in 24 (11.2%) of individuals. Those with COPD had nominally higher PDFF and EMCL but nominally lower IMCL and IMCL/EMCL ratios (Table 1).

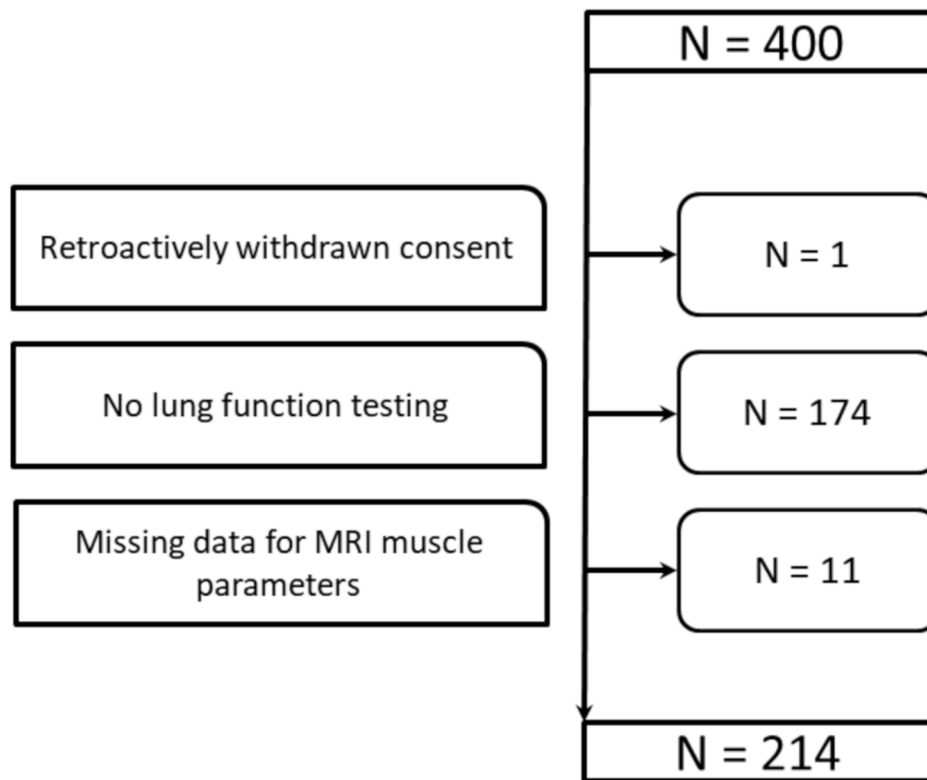
Exemplary PDFF maps are shown in Fig. 3.

Correlation between MRI-derived skeletal muscle parameters and pulmonary function

In univariate analysis, skeletal muscle and pulmonary parameters were correlated to different degrees, ranging from a Spearman correlation coefficient of -0.51 between PDFF and FVC, to a correlation coefficient of 0.59 between skeletal muscle area and TLCO (Supplementary Fig. 1). We note that particularly the IMCL/EMCL ratio showed stronger correlations with pulmonary parameters in individuals with COPD compared to individuals without COPD (Supplementary Fig. 1).

Association of MRI-derived skeletal muscle parameters with pulmonary function and COPD

After full adjustment, there were physiologically plausible associations between MRI-derived muscle area with VA (beta = 0.16, 95%CI: [0.05, 0.27], $p = 0.005$), TLC (beta = 0.16, 95%CI: [0.05, 0.27], $p = 0.004$), FVC (beta = 0.14, 95%CI: [0.02, 0.25], $p = 0.017$) and TLCO (beta = 0.20, 95%CI: [0.08, 0.32], $p = 0.001$, Fig. 4 and Supplementary Tables 2–4).

**Fig. 2** Participant Flowchart

Flowchart showing the inclusion and exclusion process for study participants. Total number of assessed participants ($n=400$) included ($n=214$), and excluded individuals with reasons for exclusion

However, there was no association between skeletal muscle areas with the presence of COPD (Table 2). PDFF was not associated with any parameter of pulmonary volume (Fig. 4, Supplementary Table 2), but an increase PDFF was tentatively associated with a decrease in FEV_1/FEV ($\beta=-0.15$, 95%CI: [-0.31, 0.01], $p=0.07$, Fig. 4 and Supplementary Table 3), as well with a decrease in TLCO ($\beta=-0.11$, 95%CI: [-0.22, 0.00], $p=0.043$) and TLCO/VA ($\beta=-0.19$, 95%CI: [-0.35, -0.04], $p=0.016$, Fig. 4 and Supplementary Table 4). An increase in one standard deviation of PDFF was associated of a 1.69 fold increase in risk for COPD ($p=0.046$, Table 2).

There were no associations of IMCL with pulmonary volumes or obstruction parameters (Fig. 4 and Supplementary Tables 2 and 3), but increased IMCL was tentatively associated with decreased TLCO/VA ($\beta=-0.14$, 95%CI: [-0.29, 0.01], $p=0.074$, Fig. 4 and Supplementary Table 4). Changes in IMCL were not associated with the presence of COPD (Table 2). EMCL showed a similar trend of associations, with a more pronounced association for the decrease in TLCO ($\beta=-0.13$, 95%CI: [-0.23, -0.03], $p=0.013$) and TCLO/VA ($\beta=-0.18$, 95%CI: [-0.33, -0.03], $p=0.022$, Fig. 4 and Supplementary Table 4). Changes in EMCL were not associated with the presence of COPD (Table 2). The ratio IMCL/EMCL was

tentatively associated with higher FEV1/FVC ($\beta=-0.12$, 95%CI: [-0.02, 0.27], $p=0.095$), as well as with higher TLCO ($\beta=0.11$, 95%CI: [0.02, 0.20], $p=0.021$) and TCLO/VA ($\beta=0.15$, 95%CI: [0.01, 0.29], $p=0.031$, Fig. 4 and Supplementary Table 4). A higher IMCL/EMCL ratio was associated with a 51% reduced risk for COPD (OR: 0.49, $p=0.050$, Table 2).

Discussion

This imaging study demonstrated that (1) myosteosis, expressed as increased PDFF in paraspinal muscles is associated with obstructive lung disease and impaired lung function parameters, (2) the distribution of fat between different compartments appears particularly relevant: a higher ratio of intramyocellular to extramyocellular lipids was associated with lower risk of obstructive lung disease, suggesting preserved metabolic function.

Several studies have demonstrated muscle alterations in individuals with COPD, with recent evidence highlighting associations between myosteosis and systemic inflammation, altered muscle bioenergetics, and adverse clinical outcomes [24–26]. Muscle dysfunction represents a well-established extrapulmonary manifestation of COPD, affecting both respiratory and locomotor muscles [4]. Robles et al. have shown that muscle fat infiltration

Table 1 Participants' clinical characteristics, muscle composition, and pulmonary function

	All N=214	No COPD (LLN) N=190	COPD (LLN) N=24	p-value
Demographics				
Age, years	58.5±5.8	58.6±5.6	57.2±6.7	0.276
Men	120 (56.1%)	104 (54.7%)	16 (66.7%)	0.373
Body Composition				
Height, cm	171.0±10.0	170.8±9.8	172.9±11.8	0.685
Weight, kg	83.8±15.9	83.9±15.8	82.5±16.5	0.330
BMI, kg/m ²	28.6±4.7	28.7±4.7	27.6±5.1	0.290
BMI ≥ 30 kg/m ²	69 (32.2%)	63 (33.2%)	6 (25.0%)	0.566
Waist circumference, cm	100.2±13.4	100.3±13.2	99.4±15.1	0.739
Body Surface Area, m ²	2.0±0.2	2.0±0.2	2.0±0.2	0.948
Lipid Profile				
Total Cholesterol, mg/dL	222.4±37.2	222.5±36.3	221.6±44.4	0.918
Triglycerides, mg/dL (median [Q1, Q3])	113.0 [83.2, 163.6]	112.5 [84.1, 154.5]	124.3 [66.5, 198.2]	0.664
HDL, mg/dL	62.2±17.7	62.7±17.8	58.4±16.6	0.267
LDL, mg/dL	142.9±34.4	143.0±33.8	142.0±39.5	0.898
Lipid lowering medication	27 (12.6%)	24 (12.6%)	3 (12.5%)	0.332
Glycemia				
Status				0.730
normoglycemia	121 (56.5%)	108 (56.8%)	13 (54.2%)	
prediabetes	60 (28.0%)	54 (28.4%)	6 (25.0%)	
diabetes	33 (15.4%)	28 (14.7%)	5 (20.8%)	
Fasting glucose, mg/dL	106.3±21.7	106.2±22.3	106.7±16.7	0.918
HbA1c, %	5.6±0.6	5.6±0.7	5.7±0.4	0.748
Glucose lowering medication	19 (8.9%)	17 (8.9%)	2 (8.3%)	0.773
Blood Pressure				
Systolic blood pressure, mmHg	122.1±16.0	121.9±15.9	123.6±17.1	0.640
Diastolic blood pressure, mmHg	76.8±9.7	77.0±9.9	74.6±7.8	0.254
Hypertension	85 (39.7%)	76 (40.0%)	9 (37.5%)	0.988
Antihypertensive medication	64 (29.9%)	59 (31.1%)	5 (20.8%)	0.427
Lifestyle Factors				
Physical Activity				0.841
regularly 2 h/w	59 (27.6%)	52 (27.4%)	7 (29.2%)	
regularly 1 h/w	69 (32.2%)	62 (32.6%)	7 (29.2%)	
sporadically	31 (14.5%)	27 (14.2%)	4 (16.7%)	
inactive	55 (25.7%)	49 (25.8%)	6 (25.0%)	
Smoking				0.485
never-smoker	82 (38.3%)	75 (39.5%)	7 (29.2%)	
ex-smoker	87 (40.7%)	77 (40.5%)	10 (41.7%)	
smoker	45 (21.0%)	38 (20.0%)	7 (29.2%)	
Inflammation				
hsCRP, mg/L (N=211)	1.2 [0.7, 2.8]	1.2 [0.7, 2.6]	1.4 [0.8, 5.7]	
Lung Volume, MRI (N=213)				
total, L	4.0±1.1	3.9±1.0	4.8±1.5	<0.001
left, L	1.8±0.6	1.8±0.5	2.2±0.7	<0.001
right, L	2.2±0.6	2.1±0.6	2.6±0.8	<0.001
Skeletal Muscle, MRI				
Area, mm ²	4945.9±1124.4	4949.1±1131.3	4920.6±1091.5	0.907
Myosteatosis, PDFF %	18.5±7.6	18.3±7.6	19.9±7.0	0.336
IMCL, % (N=206)	8.3±2.8	8.4±2.9	7.9±1.7	0.466
IMCL, %, median [Q1, Q3] (N=206)	7.8 [6.4, 9.7]	7.8 [6.3, 9.8]	7.7 [6.8, 8.4]	
EMCL, % (N=206)	9.0±5.7	9.0±5.7	9.3±5.3	0.800
EMCL, %, median [Q1, Q3] (N=206)	8.0 [4.7, 11.2]	8.0 [4.6, 11.5]	8.5 [6.4, 9.6]	

Table 1 (continued)

	All N=214	No COPD (LLN) N=190	COPD (LLN) N=24	p-value
IMCL/EMCL, (N=206)	1.2±0.6	1.2±0.6	1.0±0.4	0.135
IMCL/EMCL, median [Q1, Q3] (N=206)	1.0 [0.8, 1.4]	1.0 [0.8, 1.4]	0.9 [0.8, 1.2]	
Pulmonary function				
RV, L (N=206)	2.13±0.40	2.09±0.37	2.44±0.48	<0.001
FRC, L (N=204)	2.86±0.68	2.82±0.66	3.16±0.75	0.021
VA, L (N=206)	6.02±1.21	5.98±1.20	6.33±1.31	0.176
TLC, L (N=206)	6.20±1.22	6.16±1.21	6.51±1.32	0.184
FVC, L	4.12±1.03	4.10±1.03	4.28±1.06	0.424
FEV ₁ /FVC	74.92±7.67	76.84±5.23	59.71±6.97	<0.001
FEF _{25–75}	2.45±0.93	2.61±0.86	1.21±0.50	<0.001
TLCO, mmol/min/kPa (N=206)	8.40±1.99	8.42±1.96	8.24±2.22	0.686
TLCO/VA, mmol/min/kPa/L (N=206)	1.40±0.19	1.41±0.19	1.30±0.19	0.006

Values are presented as arithmetic means and standard deviations (or otherwise indicated) with p-values from t-test (or Mann-Whitney-U test), or counts and percentages with p-values from X²-test or Fisher's exact test

Abbreviations: BMI: body mass index; EMCL: extramyocellular lipids; FEF_{25–75}: forced expiratory flow between 25% and 75% of FVC; FEV₁/FVC: Tiffenau-Index; FRC: functional residual capacity; FVC: forced vital capacity; HbA1c: glycated hemoglobin; HDL: high density lipoprotein; hsCRP: high sensitivity C-reactive protein; IMCL: intramyocellular lipids; LDL: low density lipoprotein; MRI: magnetic resonance imaging; PDFF: proton density fat fraction; RV: residual volume; TLC: total lung capacity; TLCO: transfer factor of the lung for carbon monoxide; VA: alveolar volume

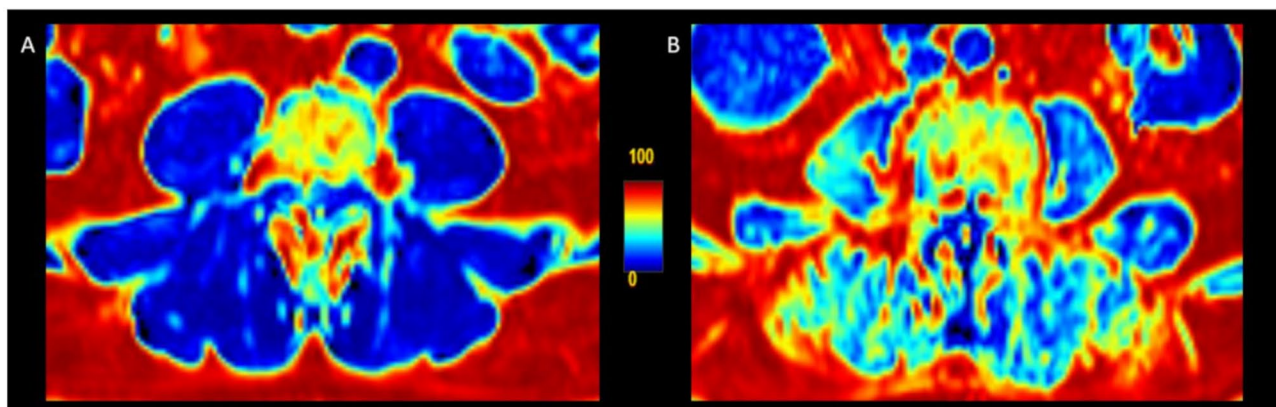


Fig. 3 Proton density fat fraction (PDFF) maps of paraspinal muscles at level L3 showing (A) low muscle fat content in an individual without COPD (PDFF 4.5%, FEV₁/FVC 70.8) and (B) high muscle fat content in an individual with COPD (PDFF 38.8%, FEV₁/FVC 54.4). Color scale indicates PDFF values from 0% (blue) to 100% (red)

Abbreviations: PDFF: proton density fat fraction; L3: 3rd lumbar vertebra; COPD: chronic obstructive pulmonary disease; FEV₁/FVC: Tiffenau-Index

is associated with impaired lower extremity muscle function in COPD patients [27]. In another study by Shields et al., increased intermuscular fat content was correlated with reduced quadriceps strength in COPD patients [28]. Population-based studies examining muscle-respiratory relationships are particularly scarce, as most evidence is derived from clinical cohorts with established diseases [29–31]. The present study extends this research by investigating associations between COPD and muscle fat composition in a general population setting, with a particular focus on IMCL and EMCL evaluation using chemical shift encoded MRI.

The role of skeletal muscle dysfunction in respiratory diseases is well-documented, yet the specific underlying processes remain incompletely understood [32].

Multiple mechanisms may link myosteatorsis to obstructive lung disease. Adipose tissue is now recognized as an endocrine organ, and ectopic fat accumulation in various compartments, including skeletal muscle, liver, and visceral adipose tissue, has been linked to metabolic disorders and obesity - conditions known to be associated with impaired respiratory function [33]. Moreover, the pro-inflammatory properties of intermuscular adipose tissue and chronic systemic inflammation in COPD may promote adipogenesis within muscle tissue, potentially contributing to a cycle of increased fat accumulation and inflammatory activity [11, 24, 34]. Further, hypoxia and oxidative stress can impair muscle metabolism and promote lipid accumulation [35], while physical inactivity due to respiratory symptoms may contribute to muscle

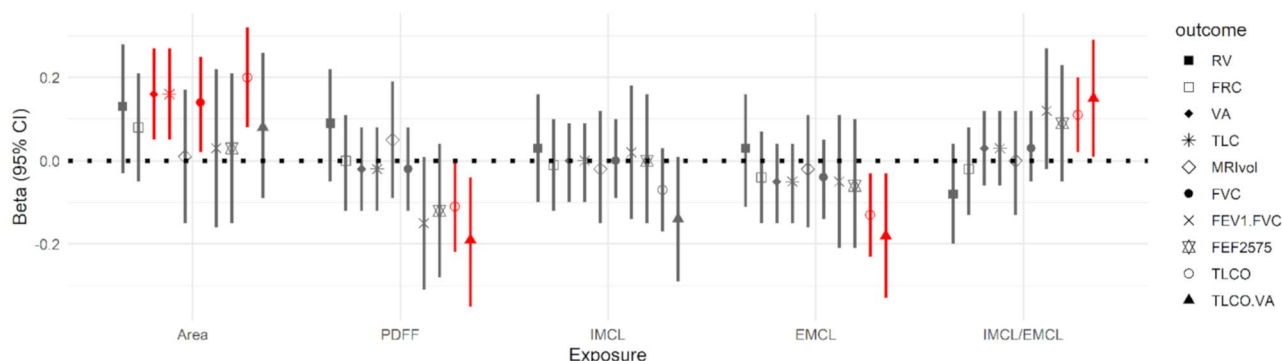


Fig. 4 Association between muscle parameters and outcomes of lung volumes, obstruction, and gas exchange Presented are beta coefficients and corresponding 95% CIs (on the y-axis) from a linear regression model with exposure muscle parameters (on the x-axis), as derived by MRI, and outcomes of pulmonary volumes, obstruction and gas exchange. Results with $p < 0.05$ are displayed in red. Presented are results from the model with full adjustment: Adjusted for age, sex, smoking, diabetes, physical activity (yes/no), and BMI. All exposures and outcomes were standardized before modelling, indicating change in the standard deviation of the pulmonary function outcome by one standard deviation change in the skeletal muscle exposure

Abbreviations: BMI: body mass index; EMCL: extramyocellular lipids; FEF_{25–75}: forced expiratory flow between 25% and 75% of FVC; FEV₁/FVC: Tiffenau-Index; FRC: functional residual capacity; FVC: forced vital capacity; IMCL: intramyocellular lipids; MRIvol: MRI (magnetic resonance imaging) derived lung volumes; PDFF: proton density fat fraction; RV: residual volume; TLC: total lung capacity; TLCO: transfer factor of the lung for carbon monoxide; VA: alveolar volume

Table 2 Association between MRI-derived skeletal muscle parameters and presence of obstructive lung disease

Exposure	Adjustment	Outcome COPD		
		OR	95%-CI	p-value
Area (mm ²)	Age + sex	0.71	[0.39, 1.27]	0.250
	Full	0.75	[0.40, 1.41]	0.368
	Full + hsCRP	0.87	[0.47, 1.63]	0.669
PDFF (%)	Age + sex	1.62	[1.01, 2.58]	0.044
	Full	1.82	[1.10, 3.02]	0.020
	Full + hsCRP	1.69	[1.01, 2.84]	0.046
IMCL (%)	Age + sex	0.97	[0.59, 1.59]	0.889
	Full	1.02	[0.61, 1.73]	0.926
	Full + hsCRP	1.05	[0.60, 1.86]	0.861
EMCL (%)	Age + sex	1.31	[0.82, 2.09]	0.259
	Full	1.44	[0.87, 2.38]	0.154
	Full + hsCRP	1.35	[0.81, 2.26]	0.252
IMCL/EMCL	Age + sex	0.52	[0.28, 0.98]	0.043
	Full	0.46	[0.23, 0.93]	0.030
	Full + hsCRP	0.49	[0.24, 1.00]	0.050

Results from a logistic regression model with exposure skeletal muscle parameters, as derived by MRI, and outcome COPD defined as FEV₁/FVC below the lower limits of normal. Full adjustment: Adjusted for age, sex, smoking, diabetes, physical activity (yes/no), and BMI. All exposures were standardized before modeling, and Odds Ratios (OR) are given per change in standard deviation

Abbreviations: BMI: body mass index; EMCL: extramyocellular lipids; FEV₁/FVC: Tiffenau-Index; IMCL: intramyocellular lipids; PDFF: proton density fat fraction

atrophy and increased fat deposition [36]. While some of these mechanisms, particularly physical inactivity, might suggest altered muscle mass in COPD, we found no significant associations between muscle area and COPD in our study. Although muscle area showed associations with lung volumes and was positively associated with gas exchange capacity — likely reflecting generally larger

body sizes — the lack of association with COPD suggests that it is not reduced muscle quantity (e.g., sarcopenia), but rather reduced muscle quality (e.g., myosteatosis) and specifically the pattern of fat distribution, that may be more relevant in obstructive respiratory disease. This is supported by our observation that while higher total myosteatosis showed negative associations, higher IMCL/EMCL ratios showed protective associations with COPD status.

The paraspinal muscles play a critical role in posture, core stability, and respiratory mechanics, with particular involvement during forced respiratory maneuvers [37]. This muscle group contains a high proportion of type I (slow-twitch) oxidative fibers, which characteristically maintain high IMCL levels for aerobic metabolism [38, 39]. In COPD, skeletal muscle may undergo adaptation toward type II (fast-twitch) fibers, which contain less IMCL than type I fibers and exhibit lower fatigue resistance. Of note, the shift towards type II fibers appears to correlate with disease severity in COPD patients [40]. Our findings of protective associations with higher IMCL/EMCL ratios suggests preserved type I fiber characteristics, supported by the concomitant finding of better gas exchange parameters - likely reflecting maintained aerobic muscle metabolism.

These observations of distinct muscle fat compositions may have clinical implications. MRI-derived muscle fat measurements could potentially serve as quantitative markers of muscle alterations in COPD [41]. Exercise-based interventions have shown positive effects on both muscle function and composition in COPD patients [36, 42, 43]. Additionally, novel pharmacotherapeutic agents with mechanisms of action specific to muscle fiber types

have been introduced [44]. Following, the potential role of IMCL/EMCL ratio as a marker of muscle adaptation warrants further investigation.

A particular strength of this study is the application of 3 Tesla MRI for muscle assessment. Previous studies predominantly used computed tomography to assess skeletal muscle alterations in COPD, primarily focusing on lower extremity muscle area with limited investigation of qualitative changes of skeletal muscle/myosteatosis [41]. Unlike computed tomography, which provides an indirect assessment of muscle fat content through radiodensity measurements, chemical shift encoded MRI using multi-echo Dixon-based sequences enables detailed tissue characterization without radiation exposure and provides precise and reproducible PDFF measurements corrected for T2* decay and other confounding effects [45–48]. Due to these advantages, PDFF has been established as an imaging biomarker for tissue fat quantification and represents the reference standard for non-invasive fat assessment [49, 50]. Analysis of paraspinal muscles was performed on axial images at the level of the third lumbar vertebra, a standardized anatomical location shown to provide validated surrogate parameters for overall body composition [51]. Recent advances in 3D whole-body MRI-based automated muscle segmentation [52] offer opportunities to extend muscle composition analysis to larger population cohorts and potentially to additional muscle groups relevant to respiratory function, although technical challenges remain for reliably quantifying structures like the diaphragm and intercostal muscles due to respiratory motion and complex anatomy [53].

Some limitations of our study should be considered. The cross-sectional design precludes causal inference regarding the temporal relationship between muscle changes and COPD development. Longitudinal studies are needed to determine whether respiratory impairment drives muscle fat infiltration, whether altered muscle metabolism contributes to respiratory dysfunction, or whether both processes occur simultaneously through shared pathophysiological mechanisms. We consider our results as first signals for a statistical association potentially reflecting a true biological pathway, but our relatively small sample size and the number of associations tested requires replication and validation in larger, external samples. COPD was defined based on spirometric indices without a physician's diagnosis. However, this approach has been widely applied and accepted in population-based studies, and by using the LLN criterion for FEV1/FVC in line with national as well as ATS/ERS recommendations, we minimized the risk of possibly inadequate classification, especially in older individuals [21, 54, 55]. Finally, direct histological validation was not available in our cohort. However, MRI-based PDFF

quantification has demonstrated excellent correlation with histopathological assessment in previous studies [56, 57].

In conclusion, this study demonstrates significant associations between increased paraspinal myosteatosis and spirometrically defined COPD in a population-based sample. The protective associations of higher IMCL/EMCL ratios may reflect preserved type I fiber characteristics, supporting the link between muscle metabolic properties and respiratory function. These observations indicate new opportunities for monitoring disease progression and developing therapeutic strategies in COPD. Larger longitudinal studies are warranted to confirm our findings and evaluate their prognostic implications and potential therapeutic applications.

Abbreviations

BMI	Body mass index
COPD	Chronic obstructive pulmonary disease
EMCL	Extramyocellular lipids
FEF _{25–75}	Forced expiratory flow between 25% and 75% of FVC
FEV1	Forced expiratory volume in 1 s
FRC	Functional residual capacity
FVC	Forced vital capacity
HbA1c	Glycated hemoglobin
HDL	High density lipoprotein
hsCRP	High sensitivity C-reactive protein
IMCL	Intramyocellular lipids
KORA	Cooperative Health Research in the Region of Augsburg
L3	3rd lumbar vertebra
LDL	Low density lipoprotein
LLN	Lower limit of normal
MRI	Magnetic resonance imaging
MRivol	MRI derived lung volumes
OR	Odds Ratio
PDFF	Proton density fat fraction
RV	Residual volume
TLC	Total lung capacity
TLCO	Transfer factor of the lung for carbon monoxide
VA	Alveolar volume

Supplementary Information

The online version contains supplementary material available at <https://doi.org/10.1186/s12931-025-03297-4>.

Supplementary Material 1

Acknowledgements

Financial support: This study was funded by the German Research Foundation (DFG, Bonn, Germany), the German Centre for Cardiovascular Disease Research (DZHK, Berlin, Germany), the German Center for Lung Research (DLZ, Gießen, Germany) and the Centre for Diabetes Research (DZD e.V., Neuherberg, Germany).

The KORA study was initiated and financed by the Helmholtz Zentrum München– German Research Center for Environmental Health, which is funded by the German Federal Ministry of Education and Research (BMBF) and by the State of Bavaria.

Author contributions

L.K., T.D., R.K., F.B. and C.L. designed the study, S.R., R.L. and A.P. performed the analysis, T.D., S.R., S.K. analyzed results, S.R., T.D. and M.J. prepared tables and figures, T.D., S.R., S.K. wrote the main manuscript text, all authors reviewed and approved the manuscript.

Funding

Open Access funding enabled and organized by Projekt DEAL. This study was funded by the German Research Foundation (DFG, Bonn, Germany), the German Centre for Cardiovascular Disease Research (DZHK, Berlin, Germany), the German Center for Lung Research (DLZ, Gießen, Germany) and the Centre for Diabetes Research (DZD e.V., Neuherberg, Germany). The KORA study was initiated and financed by the Helmholtz Zentrum München – German Research Center for Environmental Health, which is funded by the German Federal Ministry of Education and Research (BMBF) and by the State of Bavaria.

Data availability

The datasets analyzed during the current study are not publicly available due to national data protection laws, since the informed consent given by KORA study participants does not cover data posting in public databases. Data are available upon request by means of a project agreement from KORA. Requests should be sent to kora.passt@helmholtz-munich.de and are subject to approval by the KORA Board. Analysis codes are available from the authors upon reasonable request.

Declarations

Ethical approval

The Ethics committee of the Bavarian Chamber of Physicians approved the general KORA cohort studies. The Ethics Committee of the Ludwig-Maximilians University Munich (Munich, Germany) additionally approved the whole-body MRI substudy (No. 498 – 12). The study was carried out in accordance with the Declaration of Helsinki and obtained written informed consent from all participants.

Consent for publication

Not applicable.

Potential competing interests

None.

Disclosures

None.

Author details

¹Department of Diagnostic and Interventional Radiology, University Medical Center Freiburg, Faculty of Medicine, University of Freiburg, Hugstetter Strasse 55, 79106 Freiburg, Germany

²Institute and Clinic for Occupational, Social and Environmental Medicine, LMU University Hospital, LMU Munich, Munich, Germany

³Comprehensive Pneumology Center Munich (CPC-M), Member of the German Center for Lung Research (DZL), Munich, Germany

⁴Institute of Epidemiology, Helmholtz Zentrum München - German Research Center for Environmental Health (GmbH), Neuherberg, Germany

⁵Chair of Epidemiology, Institute for Medical Information Processing, Biometry and Epidemiology, Medical Faculty, Ludwig-Maximilians-Universität München, Munich, Germany

⁶Department of Radiology, LMU University Hospital, LMU Munich, Munich, Germany

⁷Department of Nuclear Medicine and Clinical Molecular Imaging, University Hospital Tuebingen, Eberhard Karls University of Tuebingen, Tuebingen, Germany

⁸Department of Diagnostic and Interventional Radiology, Eberhard Karls University of Tuebingen, Tuebingen, Germany

Received: 10 February 2025 / Accepted: 8 June 2025

Published online: 14 June 2025

References

1. Global, regional, and national deaths, prevalence, disability-adjusted life years, and years lived with disability for chronic obstructive pulmonary disease and asthma, 1990–2015: a systematic analysis for the Global Burden of Disease Study 2015. *Lancet Respiratory Medicine*. 2017;5(9):691–706.
2. Christenson SA, et al. Chronic obstructive pulmonary disease. *Lancet*. 2022;399(10342):2227–42.
3. Jaitovich A, Barreiro E. Skeletal muscle dysfunction in chronic obstructive pulmonary disease. What we know and can do for our patients. *Am J Respir Crit Care Med*. 2018;198(2):175–86.
4. Maltais F, et al. An official American thoracic society/european respiratory society statement: update on limb muscle dysfunction in chronic obstructive pulmonary disease. *Am J Respir Crit Care Med*. 2014;189(9):e15–62.
5. Benz E et al. Sarcopenia in COPD: a systematic review and meta-analysis. *Eur Respir Rev*, 2019. 28(154).
6. Nagano A, et al. Respiratory sarcopenia and sarcopenic respiratory disability: concepts, diagnosis, and treatment. *J Nutr Health Aging*. 2021;25(4):507–15.
7. Diallo TD, et al. Myosteotosis in multiple myeloma: a key determinant of survival beyond sarcopenia. *Skeletal Radiol*; 2024.
8. Engelke K, et al. Magnetic resonance imaging techniques for the quantitative analysis of skeletal muscle: state of the Art. *J Orthop Translat*. 2023;42:57–72.
9. Ahn H, et al. Updated systematic review and meta-analysis on diagnostic issues and the prognostic impact of myosteotosis: A new paradigm beyond sarcopenia. *Ageing Res Rev*. 2021;70:101398.
10. Kahn D, et al. Quantifying the inflammatory secretome of human intermuscular adipose tissue. *Physiol Rep*. 2022;10(16):e15424.
11. Dondero K, et al. The effects of myosteotosis on skeletal muscle function in older adults. *Physiol Rep*. 2024;12(9):e16042.
12. Kiefer LS, et al. Distribution patterns of intramyocellular and extramyocellular fat by magnetic resonance imaging in subjects with diabetes, prediabetes and normoglycaemic controls. *Diabetes Obes Metab*. 2021;23(8):1868–78.
13. Kiefer LS, et al. Assessment of the degree of abdominal myosteotosis by magnetic resonance imaging in subjects with diabetes, prediabetes and healthy controls from the general population. *Eur J Radiol*. 2018;105:261–8.
14. Linge J, et al. Adverse muscle composition predicts all-cause mortality in the UK biobank imaging study. *J Cachexia Sarcopenia Muscle*. 2021;12(6):1513–26.
15. Nachit M, et al. AI-based CT body composition identifies myosteotosis as key mortality predictor in asymptomatic adults. *Radiology*. 2023;307(5):e222008.
16. Bamberg F, et al. Subclinical disease burden as assessed by Whole-Body MRI in subjects with prediabetes, subjects with diabetes, and normal control subjects from the general population: the KORA-MRI study. *Diabetes*. 2017;66(1):158–69.
17. Luzak A, et al. Association of physical activity with lung function in lung-healthy German adults: results from the KORA FF4 study. *BMC Pulm Med*. 2017;17(1):215.
18. Kiefer LS, et al. Inter- and intra-observer variability of an anatomical landmark-based, manual segmentation method by MRI for the assessment of skeletal muscle fat content and area in subjects from the general population. *Br J Radiol*. 2018;91(1089):20180019.
19. Bydder M, Girard O, Hamilton G. Mapping the double bonds in triglycerides. *Magn Reson Imaging*. 2011;29(8):1041–6.
20. Mueller J, et al. Automated MR-based lung volume segmentation in population-based whole-body MR imaging: correlation with clinical characteristics, pulmonary function testing and obstructive lung disease. *Eur Radiol*. 2019;29(3):1595–606.
21. Graham BL, et al. Standardization of spirometry 2019 update. An official American thoracic society and European respiratory society technical statement. *Am J Respir Crit Care Med*. 2019;200(8):e70–88.
22. Quanjer PH, et al. Age- and height-based prediction bias in spirometry reference equations. *Eur Respir J*. 2012;40(1):190–7.
23. Stanojevic S et al. ERS/ATS technical standard on interpretive strategies for routine lung function tests. *Eur Respir J*, 2022. 60(1).
24. Persson HL, et al. Skeletal myosteotosis is associated with systemic inflammation and a loss of muscle bioenergetics in stable COPD. *J Inflamm Res*. 2022;15:4367–84.
25. Wang Y, et al. Accelerated loss of trunk muscle density and size at L1 vertebral level in male patients with COPD. *Front Endocrinol (Lausanne)*. 2022;13:1087110.
26. Nicholson JM, et al. Computed tomography-based body composition measures in COPD and their association with clinical outcomes: A systematic review. *Chron Respir Dis*. 2022;19:14799731221133387.
27. Robles PG, et al. Intramuscular fat infiltration contributes to impaired muscle function in COPD. *Med Sci Sports Exerc*. 2015;47(7):1334–41.
28. Shields GS, et al. Bioenergetics and intermuscular fat in chronic obstructive pulmonary disease-associated quadriceps weakness. *Muscle Nerve*. 2015;51(2):214–21.
29. Eagan TM, et al. Body composition and plasma levels of inflammatory biomarkers in COPD. *Eur Respir J*. 2010;36(5):1027–33.

30. Attaway AH, et al. Muscle loss phenotype in COPD is associated with adverse outcomes in the UK biobank. *BMC Pulm Med.* 2024;24(1):186.
31. Tattersall MC, et al. Skeletal muscle adiposity and lung function trajectory in the severe asthma research program. *Am J Respir Crit Care Med.* 2023;207(4):475–84.
32. Iepsen UW, Pedersen BK. Development of limb muscle dysfunction in chronic obstructive pulmonary disease: smoking, inflammation, or simply disuse?? *Am J Respir Cell Mol Biol.* 2020;62(2):134–5.
33. Krüchten RV, et al. Whole-Body MRI-Derived adipose tissue characterization and relationship to pulmonary function impairment. *Tomography.* 2022;8(2):560–9.
34. Correa-de-Araujo R, et al. Myosteatosis in the context of skeletal muscle function deficit: an interdisciplinary workshop at the National Institute on aging. *Front Physiol.* 2020;11:963.
35. Henin G, et al. Myosteatosis: diagnosis, pathophysiology and consequences in metabolic dysfunction-associated steatotic liver disease. *JHEP Rep.* 2024;6(2):100963.
36. Ramírez-Vélez R, et al. Effect of exercise on myosteatosis in adults: a systematic review and meta-analysis. *J Appl Physiol (1985).* 2021;130(1):245–55.
37. Park JW, Kweon M, Hong S. The influences of position and forced respiratory maneuvers on spinal stability muscles. *J Phys Ther Sci.* 2015;27(2):491–3.
38. Agten A, et al. The lumbar multifidus is characterised by larger type I muscle fibres compared to the erector spinae. *Anat Cell Biol.* 2020;53(2):143–50.
39. Schrauwen-Hinderling VB, et al. Intramyocellular lipid content in human skeletal muscle. *Obes (Silver Spring).* 2006;14(3):357–67.
40. Gosker HR, et al. Muscle fibre type shifting in the Vastus lateralis of patients with COPD is associated with disease severity: a systematic review and meta-analysis. *Thorax.* 2007;62(11):944–9.
41. Rozenberg D, et al. Utilization of non-invasive imaging tools for assessment of peripheral skeletal muscle size and composition in chronic lung disease: A systematic review. *Respir Med.* 2017;131:125–34.
42. Li P, et al. Effects of exercise intervention on peripheral skeletal muscle in stable patients with COPD: A systematic review and Meta-Analysis. *Front Med (Lausanne).* 2021;8:766841.
43. De Brandt J, et al. Changes in structural and metabolic muscle characteristics following exercise-based interventions in patients with COPD: a systematic review. *Expert Rev Respir Med.* 2016;10(5):521–45.
44. Maddocks M, et al. Skeletal muscle adiposity is associated with physical activity, exercise capacity and fibre shift in COPD. *Eur Respir J.* 2014;44(5):1188–98.
45. Jung M, et al. Association of lumbar vertebral bone marrow and paraspinal muscle fat composition with intervertebral disc degeneration: 3T quantitative MRI findings from the population-based KORA study. *Eur Radiol.* 2023;33(3):1501–12.
46. Bray TJ, et al. Fat fraction mapping using magnetic resonance imaging: insight into pathophysiology. *Br J Radiol.* 2018;91(1089):20170344.
47. Schneider E, et al. Long-term inter-platform reproducibility, bias, and linearity of commercial PDFF MRI methods for fat quantification: a multi-center, multi-vendor Phantom study. *Eur Radiol.* 2021;31(10):7566–74.
48. Hu HH, et al. Linearity and Bias of proton density fat fraction as a quantitative imaging biomarker: A multicenter, multiplatform, multivendor Phantom study. *Radiology.* 2021;298(3):640–51.
49. Starekova J, et al. Quantification of liver fat content with CT and MRI: state of the Art. *Radiology.* 2021;301(2):250–62.
50. Idilman IS, et al. Proton density fat fraction: magnetic resonance imaging applications beyond the liver. *Diagn Interv Radiol.* 2022;28(1):83–91.
51. Schweitzer L, et al. What is the best reference site for a single MRI slice to assess whole-body skeletal muscle and adipose tissue volumes in healthy adults? *Am J Clin Nutr.* 2015;102(1):58–65.
52. Jung M, et al. Deep learning-based body composition analysis from whole-body magnetic resonance imaging to predict all-cause mortality in a large Western population. *EBioMedicine.* 2024;110:105467.
53. Kart T, et al. Automated imaging-based abdominal organ segmentation and quality control in 20,000 participants of the UK biobank and German National cohort studies. *Sci Rep.* 2022;12(1):18733.
54. Karrasch S, et al. What is the impact of different spirometric criteria on the prevalence of spirometrically defined COPD and its comorbidities? Results from the population-based KORA study. *Int J Chron Obstruct Pulmon Dis.* 2016;11:1881–94.
55. Criée CP, et al. [Recommendations on interpretive strategies for routine lung function tests]. *Pneumologie.* 2024;78(12):1003–13.
56. Smith AC, et al. Muscle-fat MRI: 1.5 Tesla and 3.0 Tesla versus histology. *Muscle Nerve.* 2014;50(2):170–6.
57. Zhang Y, et al. Reliability of measuring the fat content of the lumbar vertebral marrow and paraspinal muscles using MRI mDIXON-Quant sequence. *Diagn Interv Radiol.* 2018;24(5):302–7.

Publisher's note

Springer Nature remains neutral with regard to jurisdictional claims in published maps and institutional affiliations.